Analysis of a Sliding Mode DC–DC Boost Converter Through LPRS of a Nonlinear Plant

Ayman AlZawaideh, *Member, IEEE*, and Igor Boiko, *Senior Member, IEEE*

***Abstract*—An exact analysis of sliding mode boost converter dynamics based on the locus of a perturbed relay system (LPRS) method is presented in this article. An LPRS representation of the dc–dc boost converter based on a full nonlinear model is developed. This is a first known attempt to apply the LPRS concept to an industrial process having a nonlinear model. The frequency and amplitude of the self-excited oscillations (chattering/ripple) are analyzed through the LPRS method. The LPRS is also used to analyze the effect of the propagation of an external disturbance (fluctuations in the source voltage). It is found that the effect of source voltage fluctuations on the system dynamics can be attributed to a combination of the effects of amplitude modulation and input signal propagation. Further, LPRS is used in the design problem of the dc–dc boost converter prototype to determine the required controller hysteresis value which ensures the desired operating switching frequency. Simulation and experimental results are presented to validate and illustrate the theoretical analysis.**

***Index Terms*—Boost converter, frequency domain analysis, hysteresis band, sliding mode control (SMC), variable structure system.**

I. Introduction

DC–DC CONVERTERS are used in various industrial applications due to their high efficiency and fast dynamic response [1]. Sliding mode control (SMC) entails discontinuous control action which is appropriate for the ON–OFF operation of power converters [2], [3]. SMC advantages include robustness and a reduced sensitivity towards parameter variations and external disturbances [4], [5].

Ideal SMC with infinite switching frequency is not attainable in practice because of unmodeled/parasitic system dynamics [6]–[8]. Realizing the switching action via an ideal nonhysteretic relay would result in having a very high uncontrollable switching frequency that would depend mainly on the parameters of the system components [6]–[8]. This leads to high switching loses and a high electromagnetic interference [9]. Hence, the switching frequency has to be controlled in practical implementation of SMC dc–dc boost converters. Hysteresis is usually introduced in the relay function to ensure the converter operation at the desired switching frequency (frequency of chattering or ripple).

There are a number of publications on design and analysis of sliding mode converters. The implementation of a two-loop controller was proposed by [10], where the outer voltage loop used a fuzzy controller, while the inner control loop utilized a sliding mode (SM) controller. The hardware prototype design used analog components for the inner loop and an 8-bit microcontroller for the fuzzy controller. The problem of switching frequency variation under the change in load or line voltage was investigated in [11]. They proposed an adaptive feedforward scheme to change the relay hysteresis under the change of supply voltage and an adaptive feedback control scheme to vary the sliding variable coefficient to maintain the designed switching frequency under load change. An SM controller designing procedure for photovoltaic applications to maximize the power point tracking is presented in [12]. A rigorous analysis of pulsewidth modulation (PWM) controlled dc–dc buck and boost converters under parameter variations was presented in [13] and [14]. The authors in [15] proposed a cascade control scheme of a buck converter having an SMC for the inner current loop and a proportional integral for the output loop to control a dc motor. A systematic design procedure for SMC boost converter with a compensating network to regulate the voltage is presented in [16]. Recent publications on the application of SMC to different industrial applications can be found in [17]–[22].

There are attempts of adaptation of the small signal modeling developed for PWM control [23]–[25] to analysis of the dynamics of SM controlled systems [26]. However, this is not a rigorous approach because it does not take into account the complex dependence of the equivalent gain on the parameters of the system and the fact that switches are organized as self-excited oscillations. In the case of a boost converter, it may give noticeable errors.

In summary, the focus of most research publications was either on the design problem or on the analysis aspect where the main objective was to study the existence and stability of the SM system, while the propagation of disturbances was not addressed to a sufficient degree.

Analysis of SMC systems can be carried out through a few existing approaches which are the classical SMC theory involving the reduced-order model for the averaged dynamics and a certain approximation for the shape of the oscillations to analyze chattering or the describing function (DF) method [27]. Because the classical SMC theory entails reduced order dynamics, it does not allow one to describe such effects as the existence of a

Manuscript received February 26, 2020; accepted March 16, 2020. Date of publication March 31, 2020; date of current version July 20, 2020. This work was supported by the Khalifa University Project CIRA-2018-104. Recommended for publication by Associate Editor C. K. Tse. *(Corresponding author: Igor Boiko.)*

The authors are with the Electrical and Computer Engineering Department, Khalifa University, Abu Dhabi, United Arab Emirates (e-mail: ayman.alzawaideh@ku.ac.ae; i.boiko@ieee.org).

Color versions of one or more of the figures in this article are available online at https://ieeexplore.ieee.org.

Digital Object Identifier 10.1109/TPEL.2020.2983596

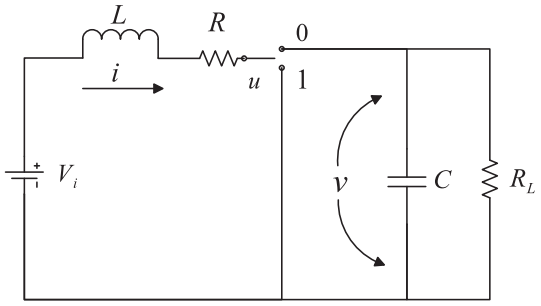

Fig. 1. Schematics of DC–DC boost converter.

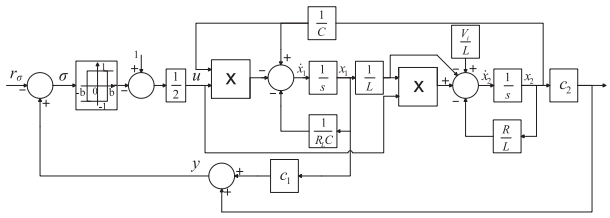

Fig. 2. SMC DC–DC boost converter block diagram.

steady-state error and the effect of fluctuations in the source voltage on the waveform of the output voltage. The DF method is based on the filtering hypothesis, and, thus, it does not provide an exact analysis [27], [28].

This article offers an analysis of SMC dc–dc boost converter dynamics using the method of the locus of a perturbed relay system (LPRS) [29], [30]. The LPRS method involves a frequency domain characteristic of the discontinuous control system that is different from Bode or Nyquist diagrams and offers an exact analysis of the periodic motion and the external signal propagation through a relay feedback system. The exact value of the equivalent gain can be also attained through the LPRS method, which can be used for the characterization of the propagation of the average error signal (on the period of oscillations) through the relay [30]. LPRS analysis of SMC dc–dc buck converter, which is a straightforward relay feedback system, was reported in [31] and [32] and that of an H-bridge inverter in [33]. However, the SMC dc–dc boost converter is a switching system but not a relay feedback system. In the previously presented research [34], [35], the equations of the boost converter were transformed into those of a relay feedback (servo) system, which was achieved through linearization carried out at the expense of disregarding the nonlinear terms in the produced equations.

In the present article, the equations of the boost converter are transformed into those of a relay servo system, without disregarding the nonlinear terms that arise in this transformation. The LPRS method for the first time is extended to analysis of a system with a nonlinear plant. Another claimed contribution of the research presented in the present article is a rigorous analysis of the effect of source voltage fluctuations (nonconstant supply voltage), specifically its representation through the effects of an amplitude modulation (AM) and input signal propagation and a rigorous analysis of both. The LPRS analysis is also used to address the design problem by providing the required value of hysteresis to be implemented in the boost converter prototype to attain the desired switching frequency.

II. SMC DC–DC Boost Converter Model

Fig. 1 depicts the dc–dc boost converter schematics, where L, C, R_L, and R are the inductance, capacitance, load resistance, and series resistance of the inductor, respectively. The source voltage is V_i, and u is the control switching signal taking a value of 1 or 0 which corresponds to closing or opening the switch, respectively.

The dynamics of the dc–dc boost converter are expressed as in [36]

$$\dot{x}_1 = -\frac{1}{R_L C}x_1 + (1-u)\frac{1}{C}x_2$$
$$\dot{x}_2 = -(1-u)\frac{1}{L}x_1 - \frac{R}{L}x_2 + \frac{V_i}{L} \tag{1}$$

where x_1 is the capacitor voltage (output voltage) and x_2 is the current through the inductor. The sliding variable is defined as in [31], which includes both the voltage and the current signals

$$\sigma = c_1(x_1 - x_{1_{ref}}) + c_2(x_2 - x_{2_{\text{ref}}}) \tag{2}$$
$$\sigma = c_1 x_1 + c_2 x_2 - r_\sigma \tag{3}$$

where $r_\sigma = c_1 x_{1_{\text{ref}}} + c_2 x_{2_{\text{ref}}}$.

The required switching frequency is obtained through introducing a hysteresis in the controller (relay action) [37]–[39]. The hysteresis band is implemented in a simple circuit that provides the following relay characteristic:

$$u = \begin{cases} 0 & \text{if } \sigma \geq b \quad \text{or } (\sigma > -b, \quad u(t-0) = 0) \\ 1 & \text{if } \sigma \leq -b \quad \text{or } (\sigma < b, \quad u(t-0) = 1) \end{cases} \tag{4}$$

where $2b$ is the value of hysteresis and $u(t-0)$ is the value of the control directly preceding the current time.

Fig. 2 depicts the SM dc–dc boost converter block diagram, where the presented model is a relay feedback system with an asymmetric relay. In order to enable the analysis of the plant dynamics using the relay system theory, the asymmetric relay requires transformation into a symmetric one, through the following substitution:

$$u = \frac{1}{2}(1 + \bar{u}) \tag{5}$$

where $\bar{\sigma} = c_1(x_{1_{\text{ref}}} - x_1) + c_2(x_{2_{\text{ref}}} - x_2)$ and the controller $\bar{u}$

$$\bar{u} = \begin{cases} 1 & \text{if } \bar{\sigma} \geq b \quad \text{or } (\bar{\sigma} > -b, \quad \bar{u}(t-0) = 1) \\ -1 & \text{if } \bar{\sigma} \leq -b \quad \text{or } (\bar{\sigma} < b, \quad \bar{u}(t-0) = -1). \end{cases}$$

The dynamics of the system in (1) can be rewritten as follows:

$$\dot{x}_1 = -\frac{1}{R_L C}x_1 + \frac{1}{2C}x_2 - \frac{1}{2C}x_2\bar{u}$$
$$\dot{x}_2 = -\frac{1}{2L}x_1 + \frac{1}{2L}x_1\bar{u} - \frac{R}{L}x_2 + \frac{V_i}{L}. \tag{6}$$

III. Transformation into Relay Servo System

The switching model of the SM boost converter (6) requires transformation into a relay servo system to be suitable for the application of the LPRS analysis on it. Hence, new variables are introduced to ensure symmetric oscillations of the states and the output signal around zero. By setting the control signal ($\bar{u}$) and the derivatives $\dot{x}_1$, $\dot{x}_2$ to zero in (6) and solving for the steady-state values one gets the following:[1]

$$x_1^* = \frac{2V_i R_L}{R_L + 4R}, x_2^* = \frac{4V_i}{R_L + 4R}.$$

Let us define new variables $\tilde{x}_1$ and $\tilde{x}_2$ being the deviation of the voltage and current, respectively, from the values of the virtual equilibrium

$$\begin{aligned}\tilde{x}_1 &= x_1 - x_1^* = x_1 - \frac{2V_i R_L}{R_L + 4R} \\ \tilde{x}_2 &= x_2 - x_2^* = x_2 - \frac{4V_i}{R_L + 4R}.\end{aligned} \tag{7}$$

Rewrite the original system model in (6) such that it includes the new states (7)

$$\begin{aligned}\dot{\tilde{x}}_1 &= -\frac{1}{R_L C}\tilde{x}_1 + \frac{1}{2C}\tilde{x}_2 - \frac{1}{2C}\bar{u}(\tilde{x}_2 + x_2^*) \\ \dot{\tilde{x}}_2 &= -\frac{1}{2L}\tilde{x}_1 - \frac{R}{L}\tilde{x}_2 + \frac{1}{2L}\bar{u}(\tilde{x}_1 + x_1^*)\end{aligned} \tag{8}$$

and the sliding variable $\tilde{\sigma} = r_\sigma - (c_1 x_1^* + c_2 x_2^*) - (c_1\tilde{x}_1 + c_2\tilde{x}_2)$

$$\tilde{\sigma} = r_\sigma - \Delta r_\sigma - \bar{y} \tag{9}$$

where the output signal $\tilde{y} = c_1\tilde{x}_1 + c_2\tilde{x}_2$ and $\Delta r_\sigma = c_1 x_1^* + c_2 x_2^*$.

Then rewriting the input signal to include the new variables

$$\tilde{r}_\sigma = r_\sigma - \Delta r_\sigma = c_1(x_{1_{\text{ref}}} - x_1^*) + c_2(x_{2_{\text{ref}}} - x_2^*). \tag{10}$$

IV. Derivation of LPRS for the Nonlinear DC–DC Boost Converter Model

To be able to analyze the periodic motion of the system represented by (8) at an unequally spaced control signal caused by having a nonzero input signal f_0, the Poincare map can be utilized.

From (8), when $\bar{u} = 1$, the converter equations may be presented in the following manner:

$$\begin{aligned}\dot{\tilde{x}}_1 &= -\frac{1}{R_L C}\tilde{x}_1 - \frac{1}{2C}x_2^* \\ \dot{\tilde{x}}_2 &= -\frac{R}{L}\tilde{x}_2 + \frac{1}{2L}x_1^*\end{aligned} \tag{11}$$

[1]Due to the existence of self-sustained oscillations, the equilibrium point does not exist in the system. Therefore, we shall call these steady-state values "virtual" because they would only occur under the assumption of $\bar{u} = 0$, which corresponds to neither opened nor closed switch.

and when $\bar{u} = -1$, they are

$$\begin{aligned}\dot{\tilde{x}}_1 &= -\frac{1}{R_L C}\tilde{x}_1 + \frac{1}{C}\tilde{x}_2 + \frac{1}{2C}x_2^* \\ \dot{\tilde{x}}_2 &= -\frac{1}{L}\tilde{x}_1 - \frac{R}{L}\tilde{x}_2 - \frac{1}{2L}x_1^*.\end{aligned} \tag{12}$$

Let ($\mathbf{A}_1$, $\mathbf{B}_1$) and ($\mathbf{A}_2$, $\mathbf{B}_2$) represent the dynamics of the system equations (11) and (12) under the control $\bar{u} = 1$ and $\bar{u} = -1$, respectively.

The plant dynamics can be represented as $\dot{\tilde{\mathbf{x}}} = \mathbf{A}_i\tilde{\mathbf{x}} + \mathbf{B}\bar{u}$ where

$$\mathbf{A}_1 = \begin{bmatrix} -\frac{1}{R_L C} & 0 \\ 0 & -\frac{R}{L} \end{bmatrix}, \quad \mathbf{A}_2 = \begin{bmatrix} -\frac{1}{R_L C} & \frac{1}{C} \\ -\frac{1}{L} & -\frac{R}{L} \end{bmatrix},$$

$$\mathbf{B} = \mathbf{B}_1 = -\mathbf{B}_2 = \begin{bmatrix} -\frac{1}{2C}x_2^* \\ \frac{1}{2L}x_1^* \end{bmatrix}.$$

The response of the linear part under a constant input is given by

$$\mathbf{x}(t) = e^{\mathbf{A}t}\mathbf{x}(0) + \mathbf{A}^{-1}\left(e^{\mathbf{A}t} - \mathbf{I}\right)\mathbf{B}\bar{u}.$$

Under the assumption of a periodic oscillation, let us write the condition of periodicity when $\bar{u} = 1$

$$\mathbf{x}(\theta_1) = e^{\mathbf{A}_1\theta_1}\mathbf{x}(0) + \mathbf{A}_1^{-1}\left(e^{\mathbf{A}_1\theta_1} - \mathbf{I}\right)\mathbf{B}$$

and when $\bar{u} = -1$

$$\mathbf{x}(\theta_1 + \theta_2) = e^{\mathbf{A}_2\theta_2}\mathbf{x}(\theta_1) - \mathbf{A}_2^{-1}\left(e^{\mathbf{A}_2\theta_2} - \mathbf{I}\right)\mathbf{B}$$

where $\mathbf{x}(0) = \mathbf{x}(\theta_1 + \theta_2)$ for a periodic solution and θ_1 and θ_2 are the positive and negative pulse duration of the control signal, respectively. The periodic motion of the SM boost converter system can be obtained through finding a fixed point of the Poincare return map

$$\begin{aligned}\mathbf{x}(0) = {} & \left[\mathbf{I} - e^{\mathbf{A}_2\theta_2}e^{\mathbf{A}_1\theta_1}\right]^{-1} \\ & \times \left[e^{\mathbf{A}_2\theta_2}\left(e^{\mathbf{A}_1\theta_1} - \mathbf{I}\right)\mathbf{A}_1^{-1} - \left(e^{\mathbf{A}_2\theta_2} - \mathbf{I}\right)\mathbf{A}_2^{-1}\right]\mathbf{B} \\ \mathbf{x}(\theta_1) = {} & \left[\mathbf{I} - e^{\mathbf{A}_1\theta_1}e^{\mathbf{A}_2\theta_2}\right]^{-1} \\ & \times \left[e^{\mathbf{A}_1\theta_1}\left(\mathbf{I} - e^{\mathbf{A}_2\theta_2}\right)\mathbf{A}_2^{-1} + \left(e^{\mathbf{A}_1\theta_1} - \mathbf{I}\right)\mathbf{A}_1^{-1}\right]\mathbf{B}.\end{aligned}$$

Now, we would like to produce the LPRS formula from the obtained Poincare map on the basis of the LPRS definition given in [28]. The imaginary part of the LPRS can be derived from the definition in [28] if we consider a symmetric oscillations as the limits $\theta_1, \theta_2 \to \theta = \frac{T}{2}$

$$\begin{aligned}\text{Im}J(\omega) &= \frac{\pi}{4}\mathbf{C}\lim_{\theta_1,\theta_2\to\theta=\frac{T}{2}}\left(\frac{x(0) - x(\theta)}{2}\right) \\ &= \frac{\pi}{8}\mathbf{C}\left[\mathbf{I} - e^{\mathbf{A}_2\theta}e^{\mathbf{A}_1\theta}\right]^{-1} \\ &\quad \times \left[e^{\mathbf{A}_2\theta}\left(e^{\mathbf{A}_1\theta} - \mathbf{I}\right)\mathbf{A}_1^{-1} - \left(e^{\mathbf{A}_2\theta} - \mathbf{I}\right)\mathbf{A}_2^{-1}\right]\mathbf{B} \\ &\quad - \left[\mathbf{I} - e^{\mathbf{A}_1\theta}e^{\mathbf{A}_2\theta}\right]^{-1} \\ &\quad \times \left[e^{\mathbf{A}_1\theta}\left(\mathbf{I} - e^{\mathbf{A}_2\theta}\right)\mathbf{A}_2^{-1} + \left(e^{\mathbf{A}_1\theta} - \mathbf{I}\right)\mathbf{A}_1^{-1}\right]\mathbf{B}.\end{aligned}$$

The switching condition of the periodic motion due to the feedback action can be represented as follows:

$$f_0 - y(0) = b$$
$$f_0 - y(\theta_1) = -b.$$

Solving for f_0 yields

$$f_0 = \frac{y(0) + y(\theta_1)}{2}$$

where f_0 is the required input signal to ensure a symmetric control signal ($u_0 = 0$). We obtain the constant term of the error signal (sliding variable) $\sigma(t)$ when $u_0 = 0$ as follows:

$$\sigma_0 = \sigma(t)|_{\theta_1=\theta_2=\frac{T}{2}} = f_0 - y_0 = \frac{y_p(0) + y_p(\theta)}{2} - y_0.$$

The real part of the LPRS can be obtained from the definition in [28] as follows:

$$\begin{aligned}\text{Re}J(\omega) &= -\frac{1}{2}\lim_{u_0\to 0}\frac{\Delta\sigma}{u_0} \\ &= -\frac{1}{2}\lim_{u_0\to 0}\frac{\sigma_{\text{avg}} - \sigma_0}{u_0} \\ &= -\frac{1}{2}\lim_{u_0\to 0}\frac{(0.5\mathbf{C}\left[\mathbf{x}(0) + \mathbf{x}(\theta_1)\right] - y_{\text{avg}}) - \sigma_0}{u_0}\end{aligned}$$

where $\Delta\sigma$ is defined as the increment of the error signal caused by the increment of u_0.

Let $\gamma = \frac{\theta_1}{\theta_1+\theta_2}, \theta_1 = \gamma T, \theta_2 = (1-\gamma), u_0 = 2\gamma - 1$.

Then the real part of the LPRS can be rewritten as follows:

$$\text{Re}J(\omega) = -\frac{1}{2}\lim_{\gamma\to\frac{1}{2}}\frac{(0.5\mathbf{C}\left[\mathbf{x}(0) + \mathbf{x}(\theta_1)\right] - y_{\text{avg}}) - \sigma_0}{2\gamma - 1}$$

and found by solving for $\frac{d\mathbf{x}(0)}{d\gamma}$, $\frac{d\mathbf{x}(\theta_1)}{d\gamma}$, and $\frac{dy_{\text{avg}}}{d\gamma}$

$$\text{Re}J(\omega) = -\frac{1}{8}\mathbf{C}\lim_{\gamma\to\frac{1}{2}}\left(\frac{d\mathbf{x}(0)}{d\gamma} + \frac{d\mathbf{x}(\theta_1)}{d\gamma}\right) + \frac{1}{4}\lim_{\gamma\to\frac{1}{2}}\frac{dy_{\text{avg}}}{d\gamma}.$$

The LPRS of the SMC dc–dc boost converter nonlinear model is as follows:

$$\begin{aligned}J(\omega) = &-\frac{1}{8}\mathbf{C}\lim_{\gamma\to\frac{1}{2}}\left(\frac{d\mathbf{x}(0)}{d\gamma} + \frac{d\mathbf{x}(\theta_1)}{d\gamma}\right) \\ &+ \frac{1}{4}\lim_{\gamma\to\frac{1}{2}}\frac{dy_{\text{avg}}}{d\gamma} + j\frac{\pi}{8}\mathbf{C}\left(\mathbf{x}(0) - \mathbf{x}(\theta)\right)\end{aligned} \tag{13}$$

where the limits of the real part are

$$\begin{aligned}&\lim_{\gamma\to\frac{1}{2}}\left(\frac{d\mathbf{x}(0)}{d\gamma}\right) \\ &= T\left[e^{-\mathbf{A}_2\theta} - e^{\mathbf{A}_1\theta}\right]^{-1}(\mathbf{A}_1 - \mathbf{A}_2)\left[e^{-\mathbf{A}_1\theta} - e^{\mathbf{A}_2\theta}\right]^{-1} \\ &\quad\times\left[e^{\mathbf{A}_2\theta}\left(e^{\mathbf{A}_1\theta} - \mathbf{I}\right)\mathbf{A}_1^{-1} - \left(e^{\mathbf{A}_2\theta} - \mathbf{I}\right)A_2^{-1}\right]\mathbf{B} \\ &\quad+\left[\mathbf{I} - e^{\mathbf{A}_2\theta}e^{\mathbf{A}_1\theta}\right]^{-1}\left[Te^{\mathbf{A}_2\theta}\left(\left(e^{\mathbf{A}_1\theta} + \mathbf{I}\right)\right.\right. \\ &\quad-\left.\left.\mathbf{A}_2\left(e^{\mathbf{A}_1\theta} - \mathbf{I}\right)\mathbf{A}_1^{-1}\right)\right]\mathbf{B}\end{aligned}$$

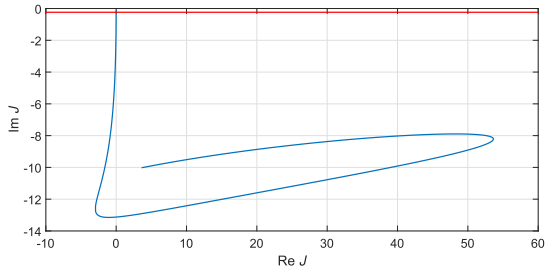

Fig. 3. SMC boost converter LPRS for the example given in Sections 6 and 7; the frequency range $\omega \in [2400, \infty]$.

$$\begin{aligned}&\lim_{\gamma\to\frac{1}{2}}\left(\frac{d\mathbf{x}(\theta_1)}{d\gamma}\right) \\ &= T\left[e^{-\mathbf{A}_1\theta} - e^{\mathbf{A}_2\theta}\right]^{-1}(\mathbf{A}_1 - \mathbf{A}_2)\left[e^{-\mathbf{A}_2\theta} - e^{\mathbf{A}_1\theta}\right]^{-1} \\ &\quad\times\left[e^{\mathbf{A}_1\theta}\left(\mathbf{I} - e^{\mathbf{A}_2\theta}\right)\mathbf{A}_2^{-1} + \left(e^{\mathbf{A}_1\theta} - \mathbf{I}\right)A_1^{-1}\right]\mathbf{B} \\ &\quad+\left[\mathbf{I} - e^{\mathbf{A}_1\theta}e^{\mathbf{A}_2\theta}\right]^{-1}\left[Te^{\mathbf{A}_1\theta}\left(\mathbf{A}_1\left(\mathbf{I} - e^{\mathbf{A}_2\theta}\right)\mathbf{A}_2^{-1}\right.\right. \\ &\quad+\left.\left.\left(e^{\mathbf{A}_2\theta} + \mathbf{I}\right)\right)\right]\mathbf{B} \\ &\lim_{\gamma\to\frac{1}{2}}\left(\frac{dy_{\text{avg}}}{d\gamma}\right) \\ &= \frac{\mathbf{C}}{T}[Te^{\mathbf{A}_1\theta}\mathbf{x}(0) - Te^{\mathbf{A}_2\theta}\mathbf{x}(\theta_1) \\ &\quad+\mathbf{A}_1^{-1}\left(e^{\mathbf{A}_1\theta} - \mathbf{I}\right)\frac{d\mathbf{x}(0)}{d\gamma} + \mathbf{A}_2^{-1}\left(e^{\mathbf{A}_2\theta} - \mathbf{I}\right)\frac{d\mathbf{x}(\theta)}{d\gamma} \\ &\quad+T\mathbf{A}_1^{-1}\left(e^{\mathbf{A}_1\theta} - \mathbf{I}\right)\mathbf{B} + T\mathbf{A}_2^{-1}\left(e^{\mathbf{A}_2\theta} - \mathbf{I}\right)\mathbf{B}]\end{aligned}$$

where $\mathbf{x}(0)$ and $\mathbf{x}(\theta_1)$ are

$$\begin{aligned}\mathbf{x}(0) = &\left[\mathbf{I} - e^{\mathbf{A}_2\theta}e^{\mathbf{A}_1\theta}\right]^{-1} \\ &\times\left[e^{\mathbf{A}_2\theta}\left(e^{\mathbf{A}_1\theta} - \mathbf{I}\right)\mathbf{A}^{-1} - \left(e^{\mathbf{A}_2\theta} - \mathbf{I}\right)\mathbf{A}_2^{-1}\right]\mathbf{B} \\ \mathbf{x}(\theta_1) = &\left[\mathbf{I} - e^{\mathbf{A}_1\theta}e^{\mathbf{A}_2\theta}\right]^{-1} \\ &\times\left[e^{\mathbf{A}_1\theta}\left(\mathbf{I} - e^{\mathbf{A}_2\theta}\right)\mathbf{A}_2^{-1} + \left(e^{\mathbf{A}_1\theta} - \mathbf{I}\right)\mathbf{A}_1^{-1}\right]\mathbf{B}.\end{aligned}$$

The derived function $J(\omega)$ (13) is defined as a characteristic of the response of the plant to the unequally spaced control signal $u(t)$, with $f_0 \to 0$ and a varying frequency ω [28]. The real part of (13) is used to find the equivalent gain, and the imaginary part of (13) contains the necessary condition for switching condition of the relay; therefore, the exact switching frequency can be found [28].

The LPRS of the dc–dc boost converter and its high-frequency component are shown in Figs. 3 and 4, respectively, for the assigned circuit parameters in Table I. From Fig. 4, the intersection point between the LPRS and the straight line at $-\frac{\pi b}{4c}$, where c is the relay amplitude which allows one to derive the exact value of the equivalent gain (k_n), an important tool for the analysis of the source voltage fluctuations and to derive the exact hysteresis value to be implemented in the controller to reflect the required switching frequency. The frequency value in the analysis problem or hysteresis value in the design problem

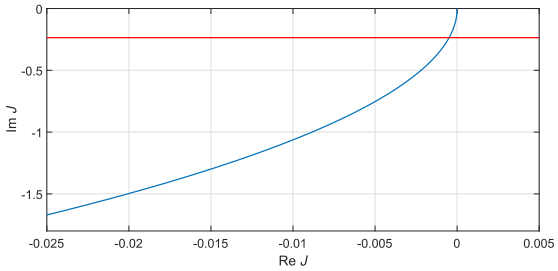

Fig. 4. LPRS high-frequency component for the example given in Sections 6 and 7.

TABLE I
PARAMETERS OF BOOST CONVERTER

Description	Parameter	Nominal Value
Input voltage	V_i [V]	22
Inductance	L [mH]	0.334
Inductor series resistance	R [Ω]	0.58
Capacitance	C [μF]	99
Load resistance	R_L [Ω]	100
Switching frequency	f [kHz]	50
Desired output voltage	V_{out} [V]	43
Hysteresis	b [V]	0.30

can be attained through solving

$$\mathrm{Im}J(\Omega) = -\frac{\pi b}{4c} \tag{14}$$

where either Ω or b is considered known, respectively. The equivalent gain of the relay may be calculated via

$$k_n = -\frac{1}{2\mathrm{Re}J(\Omega)} \tag{15}$$

which can be used for analysis of external signals propagation as shown in the following.

V. Source Voltage Fluctuation Effect

The effect of input voltage fluctuations on the inductor current or on the output voltage can be examined using LPRS method [31]. The source voltage fluctuations can be a result of rectification of the ac voltage at 50 or 60 Hz, which would result in having a 100- or 120-Hz input voltage fluctuations to the dc–dc boost converter. Therefore, the fluctuations are of a frequency much lower compared to the controller switching frequency. The corresponding condition allows one to utilize the notion of the equivalent gain to describe the effect of propagation of the source voltage fluctuations on the system dynamics. The source voltage fluctuations may be depicted via the summation of a constant (dc) signal and a periodic term

$$V_i(t) = V_{i_0} + a_E \sin(\omega_E t), \omega_E \ll \Omega \tag{16}$$

where V_{i_0} is the nominal source voltage (dc), a_E is the source voltage fluctuations amplitude, and ω_E is the fluctuations frequency of the source voltage. The effect of source voltage fluctuations ($V_i(t)$) may be attributed to a combination of the input signal propagation (10) effect and the AM effect.

A. Effect of Propagation

The original control system in (8) can be rewritten for the analysis of the slow components terms as follows:

$$\begin{aligned}\dot{\tilde{x}}_{10} &= -\frac{1}{R_L C}\tilde{x}_{10} + \frac{1}{2C}\tilde{x}_{20} - \frac{1}{2C}\bar{u}_0 x_2^* - \frac{1}{2C}\bar{u}_0\tilde{x}_{20} \\ \dot{\tilde{x}}_{20} &= -\frac{1}{2L}\tilde{x}_{10} - \frac{R}{L}\tilde{x}_{20} + \frac{1}{2L}\bar{u}_0 x_1^* + \frac{1}{2L}\bar{u}_0\tilde{x}_{10}\end{aligned} \tag{17}$$

where

$$\begin{aligned}\bar{u}_0 &= \alpha_u + a_u \sin(\omega_E t) \\ \tilde{x}_{10} &= \alpha_1 + a_{x_1}\sin(\omega_E t + \phi_1) \\ \tilde{x}_{20} &= \alpha_2 + a_{x_2}\sin(\omega_E t + \phi_2).\end{aligned} \tag{18}$$

The multiplication of the propagation of the states with the control signal

$$\begin{aligned}\tilde{x}_{10}\bar{u}_0 &= \frac{1}{2}a_u a_{x_1}\left(\cos(\phi_1) - \cos(2\omega_E t + \phi_1)\right) \\ \tilde{x}_{20}\bar{u}_0 &= \frac{1}{2}a_u a_{x_2}\left(\cos(\phi_2) - \cos(2\omega_E t + \phi_2)\right).\end{aligned} \tag{19}$$

Disregarding the terms containing $2\omega_E t$ and assuming they are of low magnitude and are filtered out, one can rewrite (19) as follows:

$$\begin{aligned}M_1 = \tilde{x}_{10}\bar{u}_0 &= \frac{1}{2}a_u a_{x_1}\cos(\phi_1) \\ M_2 = \tilde{x}_{20}\bar{u}_0 &= \frac{1}{2}a_u a_{x_2}\cos(\phi_2).\end{aligned} \tag{20}$$

Rewrite (17) to include (20)

$$\begin{aligned}\dot{\tilde{x}}_{10} &= -\frac{1}{R_L C}\tilde{x}_{10} + \frac{1}{2C}\tilde{x}_{20} - \frac{1}{2C}x_2^*\bar{u}_0 - \frac{1}{2C}M_2 \\ \dot{\tilde{x}}_{20} &= -\frac{1}{2L}\tilde{x}_{10} - \frac{R}{L}\tilde{x}_{20} + \frac{1}{2L}x_1^*\bar{u}_0 + \frac{1}{2L}M_1.\end{aligned} \tag{21}$$

The constant terms in (21) are transposed to the input signal by setting $\bar{u}_0 = 0$ and solving for the states' steady-state values

$$\tilde{x}_{10}^* = \frac{R_L(M_1 - 2RM_2)}{R_L + 4R}, \tilde{x}_{20}^* = \frac{2M_1 + R_L M_2}{R_L + 4R}.$$

Introduce new variables $\bar{x}_{10}$ and $\bar{x}_{20}$

$$\begin{aligned}\bar{x}_{10} &= \tilde{x}_{10} - \tilde{x}_{10}^* \\ \bar{x}_{20} &= \tilde{x}_{20} - \tilde{x}_{20}^*.\end{aligned} \tag{22}$$

Rewriting (21) to incorporate the introduced variables (22)

$$\begin{aligned}\dot{\bar{x}}_{10} &= -\frac{1}{R_L C}\bar{x}_{10} + \frac{1}{2C}\bar{x}_{20} - \frac{1}{2C}x_2^*\bar{u}_0 \\ \dot{\bar{x}}_{20} &= -\frac{1}{2L}\bar{x}_{10} - \frac{R}{L}\bar{x}_{20} + \frac{1}{2L}x_1^*\bar{u}_0.\end{aligned} \tag{23}$$

Analysis of the propagation of the slow signals in the converter can now be done by using the new states ($\dot{\bar{x}}_{10}$ and $\dot{\bar{x}}_{20}$), where

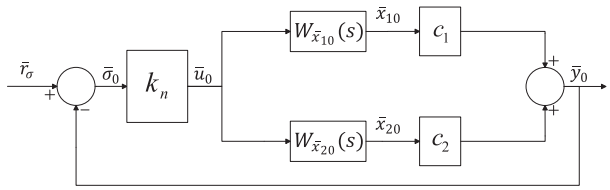

Fig. 5. Slow motion dynamics of SM boost converter.

the new input signal is

$$\begin{aligned}\bar{r}_\sigma &= r_\sigma - \Delta r_\sigma - (c_1\tilde{x}_{10}^* + c_2\tilde{x}_{20}^*)\\ &= c_1\left(\frac{2V_{i_0}R_L}{R_L+4R} - \frac{2V_iR_L}{R_L+4R}\right)\\ &\quad + c_2\left(\frac{4V_{i_0}}{R_L+4R} - \frac{4V_i}{R_L+4R}\right) - (c_1\tilde{x}_{10}^* + c_2\tilde{x}_{20}^*)\\ &= -2a_E\sin(\omega_E t)\left[\frac{c_1R_L+2c_2}{R_L+4R}\right] - (c_1\tilde{x}_{10}^* + c_2\tilde{x}_{20}^*).\end{aligned} \tag{24}$$

Thus, the dynamics of the plant can be presented as follows:

$$\dot{\tilde{\mathbf{x}}} = \mathbf{A}\bar{\mathbf{x}} + \mathbf{B}\bar{u}$$
$$\bar{y} = \mathbf{C}\bar{\mathbf{x}}$$

where the output signal is defined as $\bar{y}_0 = c_1\bar{x}_{10} + c_2\bar{x}_{20}$, and the matrices describing the SM boost converter slow signal model are

$$\mathbf{A} = \begin{bmatrix} -\frac{1}{R_LC} & \frac{1}{2C} \\ -\frac{1}{2L} & -\frac{R}{L}\end{bmatrix}, \mathbf{B} = \begin{bmatrix} -\frac{1}{2C}x_2^* \\ \frac{1}{2L}x_1^*\end{bmatrix}$$
$$\mathbf{C} = \begin{bmatrix} c_1 & c_2\end{bmatrix}.$$

The propagation of external signals through the relay servo system can be analyzed via the replacement of the conventional relay in the original system with the equivalent gain [28]. The block diagram of the SMC boost converter slow motion dynamics is presented in Fig. 5, where $W_{\bar{x}_{10}}(s)$ and $W_{\bar{x}_{20}}(s)$ are the transfer functions from the relay output to the states $\bar{x}_{10}$ and $\bar{x}_{20}$, respectively

$$W_{\bar{x}_{10}}(s) = \frac{2R_LV_i[R_L - 4(R+Ls)]}{(R_L+4R)(4LR_LCs^2 + 4R_LRCs + 4Ls + R_L + 4R)} \tag{25}$$

$$W_{\bar{x}_{20}}(s) = \frac{4R_LV_i\left[1 + (R_LCs+1)\right]}{(R_L+4R)(4LR_LCs^2 + 4R_LRCs + 4Ls + R_L + 4R)}. \tag{26}$$

Once the relay nonlinearity is substituted with the equivalent gain, the closed-loop transfer functions of the controlled system can be written, where the transfer functions from the set point to the output voltage and inductor current deviations represented by $W_{\bar{r}_\sigma\to\bar{x}_{10}}(s)$ and $W_{\bar{r}_\sigma\to\bar{x}_{20}}(s)$ are written as follows:

$$\begin{aligned}W_{\bar{r}_\sigma\to\bar{x}_{10}}(s) &= \frac{k_nW_{\bar{x}_{10}}(s)}{1 + k_n\left(c_1W_{\bar{x}_{10}}(s) + c_2W_{\bar{x}_{20}}(s)\right)}.\\ W_{\bar{r}_\sigma\to\bar{x}_{20}}(s) &= \frac{k_nW_{\bar{x}_{20}}(s)}{1 + k_n\left(c_1W_{\bar{x}_{10}}(s) + c_2W_{\bar{x}_{20}}(s)\right)}.\end{aligned} \tag{27}$$

The transfer function from the input signal to the output signal $\bar{y}_0$ is as follows:

$$W_{\bar{r}_\sigma\to\bar{y}_0}(s) = \frac{k_n\left(c_1W_{\bar{x}_{10}}(s) + c_2W_{\bar{x}_{20}}(s)\right)}{1 + k_n\left(c_1W_{\bar{x}_{10}}(s) + c_2W_{\bar{x}_{20}}(s)\right)}. \tag{28}$$

The fluctuations of the states ($\tilde{x}_{10}$ and $\tilde{x}_{20}$) due to the propagation effect are

$$\begin{aligned}\tilde{x}_{10} = &-2a_E\left[\frac{c_1R_L+2c_2}{R_L+4R}\right]|W_{\bar{r}_\sigma\to\bar{x}_{10}}(j\omega_E)|\\ &\times\sin\left(\omega_Et + \arg W_{\bar{r}_\sigma\to\bar{x}_{10}}(j\omega_E)\right)\\ &-(c_1\tilde{x}_{10}^* + c_2\tilde{x}_{20}^*)\frac{k_nW_{\bar{x}_{10}}(0)}{1 + k_n\left(c_1W_{\bar{x}_{10}}(0) + c_2W_{\bar{x}_{20}}(0)\right)} + \tilde{x}_{10}^*\end{aligned} \tag{29}$$

$$\begin{aligned}\tilde{x}_{20} = &-2a_E\left[\frac{c_1R_L+2c_2}{R_L+4R}\right]|W_{\bar{r}_\sigma\to\bar{x}_{20}}(j\omega_E)|\\ &\times\sin\left(\omega_Et + \arg W_{\bar{r}_\sigma\to\bar{x}_{20}}(j\omega_E)\right)\\ &-(c_1\tilde{x}_{10}^* + c_2\tilde{x}_{20}^*)\frac{k_nW_{\bar{x}_{10}}(0)}{1 + k_n\left(c_1W_{\bar{x}_{10}}(0) + c_2W_{\bar{x}_{20}}(0)\right)} + \tilde{x}_{20}^*\end{aligned} \tag{30}$$

and the fluctuations of the control signal due to propagation effect is

$$\tilde{u}_0 = -k_n\left[2a_E\left[\frac{c_1R_L+2c_2}{R_L+4R}\right]\sin(\omega_Et) + (c_1\tilde{x}_{10} + c_2\tilde{x}_{20})\right]. \tag{31}$$

Solving (29)–(31) would allow one to find the variables in (18).

The fluctuations of the voltage and the current as a result of the propagation effect is

$$\delta_{\tilde{x}_{10}\text{Prop}} = \tilde{x}_{10} + \frac{2V_iR_L}{R_L+4R} \tag{32}$$

$$\delta_{\tilde{x}_{20}\text{Prop}} = \tilde{x}_{20} + \frac{4V_i}{R_L+4R}. \tag{33}$$

B. Propagation of Amplitude-Modulated Signal Through Linear Dynamics

Another component arising from the fluctuating source voltage can be described as AM. Consider the following model showing how an amplitude-modulated signal propagates through linear dynamics. Assume that a carrier signal $u(t)$ is modulated by signal $V(t)$ and the modulated signal propagates through the linear dynamics with transfer function $G(s)$, as shown in Fig. 6, where

$$u(t) = a_c\sin(\Omega t) \tag{34}$$

$$V(t) = 1 + \alpha_m\sin(\omega_m t), \quad \omega_m \ll \Omega. \tag{35}$$

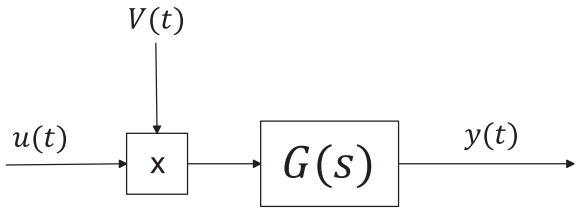

Fig. 6. Propagation of amplitude modulated signal through linear dynamics.

The product of the carrier and the modulation signals is

$$\begin{aligned} u(t)V(t) &= a_c\sin(\Omega t)(1+\alpha_m\sin(\omega_m t)) \\ &= a_c\sin(\Omega t) + \frac{a_c\alpha_m}{2}[\cos((\Omega-\omega_m)t) \\ &\quad - \cos((\Omega+\omega_m)t)]. \end{aligned} \tag{36}$$

Due to the fact that $\omega_m \ll \Omega$, $\Omega-\omega_m$, and $\Omega+\omega_m$ can be considered as small deviations from Ω, we can use the following linear approximations:

$$M(\Omega+\omega_m) = M(\Omega) + \left.\frac{\partial M}{\partial \omega}\right|_{\omega=\Omega}\omega_m \tag{37}$$

$$M(\Omega-\omega_m) = M(\Omega) - \left.\frac{\partial M}{\partial \omega}\right|_{\omega=\Omega}\omega_m \tag{38}$$

where

$$M(\omega) = |G(j\omega)| \tag{39}$$

is the magnitude characteristic of linear dynamics and

$$\varphi(\Omega+\omega_m) = \varphi(\Omega) + \left.\frac{\partial \varphi}{\partial \omega}\right|_{\omega=\Omega}\omega_m \tag{40}$$

$$\varphi(\Omega-\omega_m) = \varphi(\Omega) - \left.\frac{\partial \varphi}{\partial \omega}\right|_{\omega=\Omega}\omega_m \tag{41}$$

where

$$\varphi(\omega) = arg(G(j\omega)) \tag{42}$$

is the phase characteristic of the linear dynamics. Using expansion (36), we shall find the propagation of each frequency separately (of the carrier frequency Ω, lower side frequency $\Omega-\omega_m$, and upper side frequency $\Omega+\omega_m$) and then sum the responses together. The output is

$$\begin{aligned} y(t) &= Ma_c\sin(\Omega t+\varphi) \\ &\quad + \frac{a_c\alpha_m}{2}[(M-\Delta M)\cos((\Omega-\omega_m)t+\varphi-\Delta\varphi) \\ &\quad - (M+\Delta M)\cos((\Omega-\omega_m)t+\varphi+\Delta\varphi)] \end{aligned} \tag{43}$$

where

$$M = M(\Omega),\ \Delta M = \left.\frac{\partial M}{\partial \omega}\right|_{\omega=\Omega}\omega_m$$

$$\varphi = \arg(G(j\Omega)),\ \Delta\varphi = \left.\frac{\partial \varphi}{\partial \omega}\right|_{\omega=\Omega}\omega_m.$$

In (43), consider the angles under cos as a sum of $\Delta\varphi$ and the rest of the expression and use the formula for the cos of a sum

$$\begin{aligned} y(t) &= Ma_c\sin(\Omega t+\varphi) \\ &\quad + \frac{a_c\alpha_m}{2}\{M\cos((\Omega-\omega_m)t+\varphi)\cos(\Delta\varphi) \\ &\quad + M\sin((\Omega-\omega_m)t+\varphi)\sin(\Delta\varphi) \\ &\quad - \Delta M\cos((\Omega-\omega_m)t+\varphi)\cos(\Delta\varphi) \\ &\quad - \Delta M\sin((\Omega-\omega_m)t+\varphi)\sin(\Delta\varphi) \\ &\quad - M\cos((\Omega+\omega_m)t+\varphi)\cos(\Delta\varphi) \\ &\quad + M\sin((\Omega+\omega_m)t+\varphi)\sin(\Delta\varphi) \\ &\quad - \Delta M\cos((\Omega+\omega_m)t+\varphi)\cos(\Delta\varphi) \\ &\quad + \Delta M\sin((\Omega+\omega_m)t+\varphi)\sin(\Delta\varphi)\} \\ &= Ma_c\sin(\Omega t+\varphi) + \frac{a_c\alpha_m}{2} \\ &\quad \times \{M\cos(\Delta\varphi)[\cos((\Omega-\omega_m)t+\varphi) \\ &\quad - \cos((\Omega+\omega_m)t+\varphi)] \\ &\quad + M\sin(\Delta\varphi)[\sin((\Omega-\omega_m)t+\varphi) \\ &\quad + \sin((\Omega+\omega_m)t+\varphi)] \\ &\quad - \Delta M\cos(\Delta\varphi)[\cos((\Omega-\omega_m)t+\varphi) \\ &\quad + \cos((\Omega+\omega_m)t+\varphi)] \\ &\quad - \Delta M\sin(\Delta\varphi)[\sin((\Omega-\omega_m)t+\varphi) \\ &\quad - \sin((\Omega+\omega_m)t+\varphi)]\} \\ &= Ma_c\sin(\Omega t+\varphi) \\ &\quad + \frac{a_c\alpha_m}{2}\{M\cos(\Delta\varphi)2\sin(\Omega t+\varphi)\sin(\omega_m t) \\ &\quad + M\sin(\Delta\varphi)2\sin(\Omega t+\varphi)\cos(\omega_m t) \\ &\quad - \Delta M\cos(\Delta\varphi)2\cos(\Omega t+\varphi)\cos(\omega_m t) \\ &\quad + \Delta M\sin(\Delta\varphi)2\cos(\Omega t+\varphi)\sin(\omega_m t)\} \\ &= Ma_c\sin(\Omega t+\varphi)\{1+\alpha_m\sin(\omega_m t)\cos(\Delta\varphi) \\ &\quad + \alpha_m\cos(\omega_m t)\sin(\Delta\varphi)\} \\ &\quad + a_c\alpha_m\Delta M\cos(\Omega t+\varphi)\{\cos(\omega_m t)\cos(\Delta\varphi) \\ &\quad + \sin(\omega_m t)\sin(\Delta\varphi)\} \\ &= y_p(t)\{1+\alpha_m\sin(\omega_m t+\Delta\varphi)\} \\ &\quad - a_c\alpha_m\Delta M\cos(\Omega t+\varphi)\cos(\omega_m t+\Delta\varphi) \end{aligned} \tag{44}$$

where $y_p(t) = Ma_c\sin(\Omega t+\varphi)$ is a result of propagation of $u(t)$ through the linear dynamics $G(s)$.

Denote a conjugate signal to $y_p(t)$ as follows:

$$y_p^*(t) = Ma_c\cos(\Omega t+\varphi) \tag{45}$$

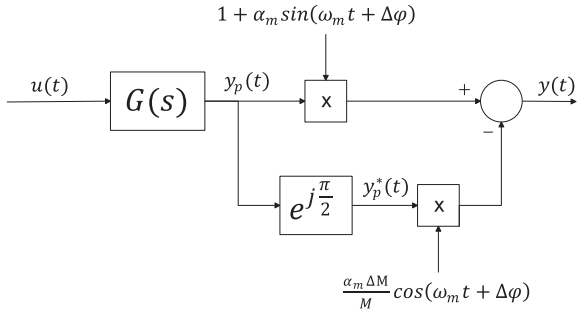

Fig. 7. Equivalent amplitude modulation diagram.

Then (44) can be rewritten as follows:

$$y(t) = y_p(t)\{1+\alpha_m \sin(\omega_m t+\Delta\varphi)\} - \frac{\alpha_m \Delta M}{M} y_p^*(t)\cos(\omega_m t+\Delta\varphi). \tag{46}$$

Considering that $y_p^*(t)$ is produced as $y_p(t)$ shifted by $\frac{\pi}{2}$, we can represent the equivalent AM diagram, where AM is applied at the output of the linear dynamics as represented in Fig. 7.

Therefore, the resulting modulated signal $y(t)$ has the following two components:

1) a result of AM by $(1+\alpha_m \sin(\omega_m t+\Delta\varphi))$ applied to the propagation through $G(s)$ signal $u(t)$;
2) a result of AM by $(\frac{\alpha_m \Delta M}{M}\cos(\omega_m t+\Delta\varphi))$ applied to $y_p^*(t)$.

The upper envelop (AM) of (46) is a result of quadratic summation of the two components (because their carriers are shifted by $\frac{\pi}{2}$)

$$y_{\text{env}}(t) = \left\{ (1+\alpha_m \sin(\omega_m t+\Delta\varphi))^2 + \left(\frac{\alpha_m \Delta M}{M}\cos(\omega_m t+\Delta\varphi)\right)^2 \right\}^{1/2}. \tag{47}$$

1) Propagation of Amplitude-Modulated Signal Through Converter Dynamics: To apply the derived formulas (46) and (47) to the dc–dc boost converter dynamics, we linearize the state equations in (8) (by removing the nonlinear terms in them as they have a smaller magnitude compared to the other terms added to them), which would allow us to observe the influence of propagation of the AM throughout the investigated system. The dynamics of the system dynamics can be written as follows:

$$\begin{aligned} \dot{\tilde{x}}_1 &= -\frac{1}{R_L C}\tilde{x}_1 + \frac{1}{2C}\tilde{x}_2 - \frac{1}{2C}x_2^*\bar{u} \\ \dot{\tilde{x}}_2 &= -\frac{1}{2L}\tilde{x}_1 - \frac{R}{L}\tilde{x}_2 + \frac{1}{2L}x_1^*\bar{u}. \end{aligned} \tag{48}$$

Let $W_{x_1}(s)$ and $W_{x_2}(s)$ represent the transfer functions from the relay output to the states $\tilde{x}_1$ and $\tilde{x}_2$, respectively. Since the matrices representing the dynamics of (48) are the same as in (23), $W_{x_1}(s)$ and $W_{x_2}(s)$ are equal to (25) and (26), respectively. The presence of the input voltage V_i in the transfer functions ($W_{x_1}(s)$ and $W_{x_2}(s)$) give rise to the AM effect. The derived formula (47) can be used to find the effect of AM on the boost converter dynamics where $\alpha_m = \frac{a_E}{V_i}$, $\omega_m = 2\pi\cdot 100$, and (Ma_c) is the amplitude of chattering.

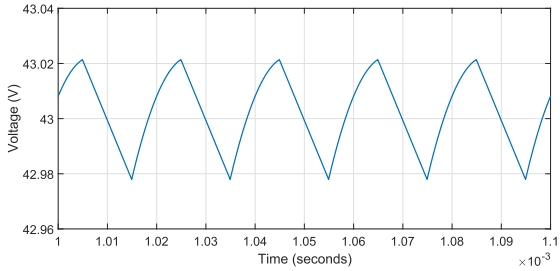

Fig. 8. Output voltage simulated waveform at steady oscillatory mode.

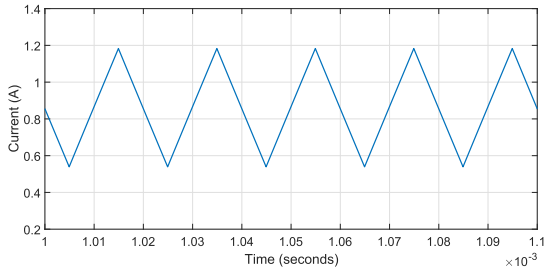

Fig. 9. Inductor current simulated waveform at steady oscillatory mode.

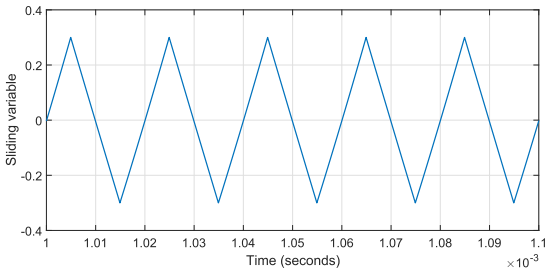

Fig. 10. Sliding variable simulated waveform at steady oscillatory mode.

VI. Simulation

Controller performance and the derived analytical equations are verified via MATLAB/Simulink simulations. Table I shows the boost converter parameters. The steady-state oscillations of the output voltage, inductor current, and the sliding variable are depicted through Figs. 8–10. The oscillations amplitude of the sliding variable is equal to the designed controller hysteresis (Table I), and the assigned inductor current reference ($I_{\text{ref}} = 0.86$ A) and output voltage reference ($V_{\text{out}} = 43.0$ V) match the simulation results. The predefined inductor current and output voltage reference values (7) are selected to ensure a symmetric controller signal action ($\theta_1 = \theta_2 = T/2$) with the desired switching frequency (50 kHz).

A. Simulation Results of the Source Voltage Fluctuations Effect

The source voltage fluctuation effects on the inductor current and the output voltage waveform are simulated in this

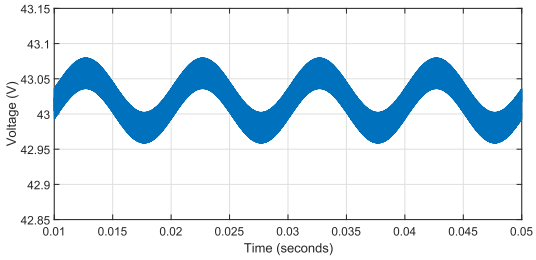

Fig. 11. Output voltage waveform due to fluctuating input voltage.

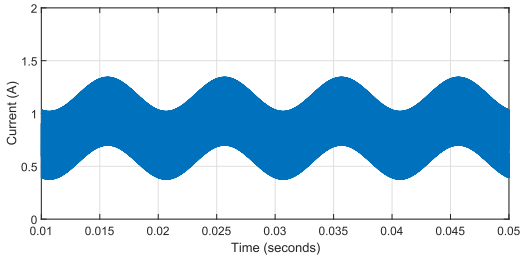

Fig. 12. Inductor current waveform due to fluctuating input voltage.

TABLE II
OSCILLATIONS PARAMETERS OF THE NONLINEAR DC–DC BOOST CONVERTER MODEL

	Magnitude
Amplitude of voltage chattering/ripple [V]	0.0217
Amplitude of current chattering/ripple [A]	0.3218
Amplitude of current AM component $\frac{a_0 a_E}{V_{i_0}}$ [A]	0.0110
Amplitude of voltage AM component $\frac{a_0 a_E}{V_{i_0}}$ [V]	0.00074
Equivalent gain k_n	1024.4
Current fluctuations amplitude due to propagation [A]	0.1616
Voltage fluctuations amplitude due to propagation [V]	0.0387

section. The frequency of the source voltage fluctuations is $w_E = 628.3$ rad/s (100 Hz), which is the result of rectification of 50 Hz input ac voltage, and the fluctuation amplitude is $a_E = 0.75$ V. The superposition principle is applied to find the combined effect of AM and propagation. The upper boundary of the propagation effect (32) is in phase with the AM effect (46), and the lower boundary of the propagation effect is in counter phase with the AM effect. Thus, the upper envelop of the combined effect has a larger magnitude compared with the lower one. The upper envelop amplitude is equal to $a_H = a_\delta + \frac{a_0 a_E}{V_{i_0}}$; however, the lower boundary amplitude is $a_L = a_\delta - \frac{a_0 a_E}{V_{i_0}}$. The effect of source voltage fluctuations on the output voltage and the inductor current waveform are shown in Figs. 11 and 12, respectively, which matches the analytical results depicted in Table II.

VII. HARDWARE IMPLEMENTATION

Verification of the derived analysis through experimental implementation is done in this section. The overall setup schematics of the SMC dc–dc boost converter and the signal description

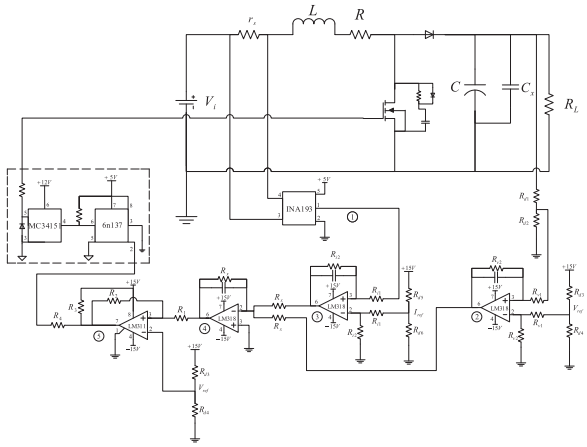

Fig. 13. Circuit schematics of SM of boost converter.

TABLE III
SIGNALS DESCRIPTION

	Magnitude
1	i_L
2	$c_1\left(x_1 - x_{1_{ref}}\right)$
3	$c_2\left(x_2 - x_{2_{ref}}\right)$
4	$c_1\left(x_{1_{ref}} - x_1\right) + c_2\left(x_{2_{ref}} - x_2\right)$
5	u

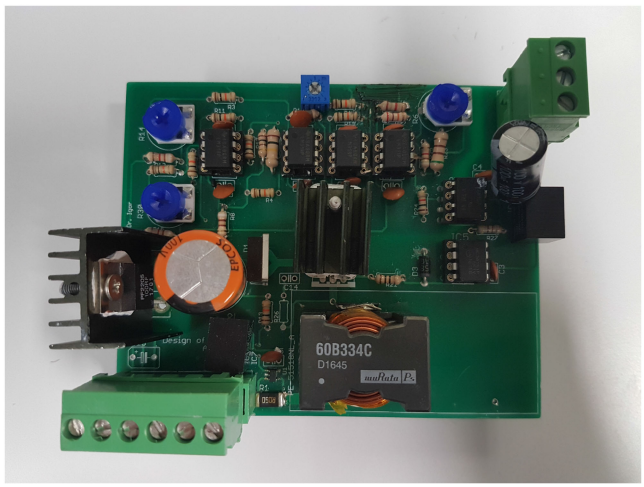

Fig. 14. Printed circuit board (PCB) of SMC boost converter.

are shown in Fig. 13 and Table III, respectively. Three operational amplifiers are used to generate the sliding variable signal $\bar{\sigma}$, which is fed to a non-inverting Schmitt trigger. The resulting signal goes to the digital circuit consisting of an opto-coupler and a MOSFET gate driver.

A. Experimental Results

The designed circuit (Fig. 13) performance is evaluated in this section. Fig. 14 depicts the prototype of the SMC dc–dc boost converter circuit, with all relevant circuit parameters presented in

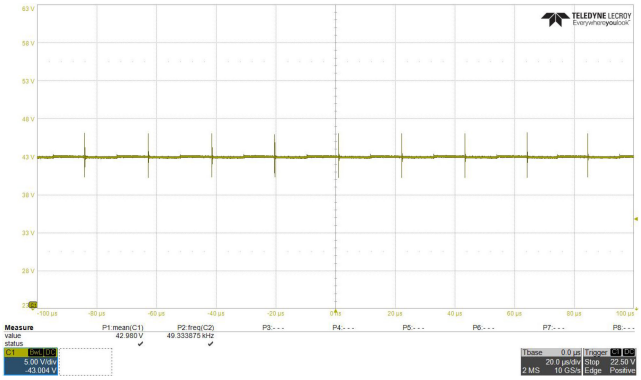

Fig. 15. Steady oscillatory operation of the output voltage, switching frequency $f = 49.33$ kHz, and average voltage $V_{\text{out}} = 42.98$ V. Each vertical division is 5 V, and each horizontal division is 20 μs.

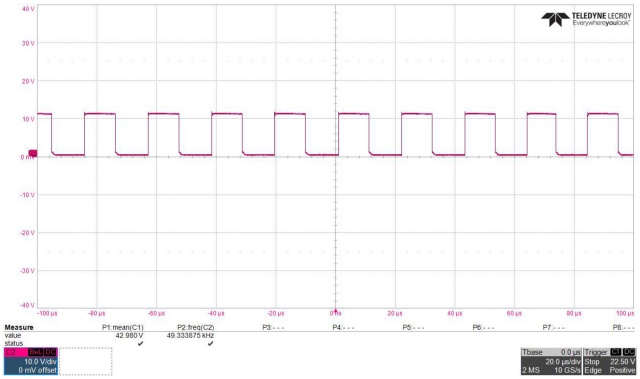

Fig. 16. Gate signal of the MOSFET, switching frequency $f = 49.33$ kHz. Each vertical division is 10 V, and each horizontal division is 20 μs.

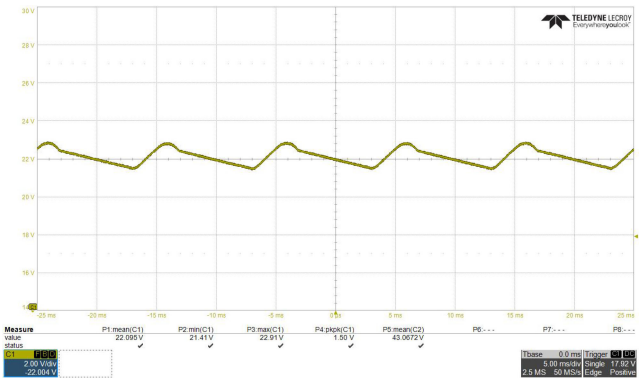

Fig. 17. Source voltage fluctuations, amplitude of fluctuations $a_E = 0.75$ V, fluctuations frequency $f = 100$ Hz. Each vertical division is 2 V, and each horizontal division is 5 ms.

Table I. The hysteresis value is calculated and set to such a value that the circuit would operate at 50 kHz. Figs. 15 and 16 show the output voltage ripple and the gate switching signal at the steady-state operation, respectively. The output voltage average value is 42.98 V, and the operating switching frequency is 49.33 kHz. The effect of source voltage fluctuations (at 100 Hz) given in Fig. 17 on the output voltage waveform is shown in Fig. 18. The analytical and experimental results are presented in

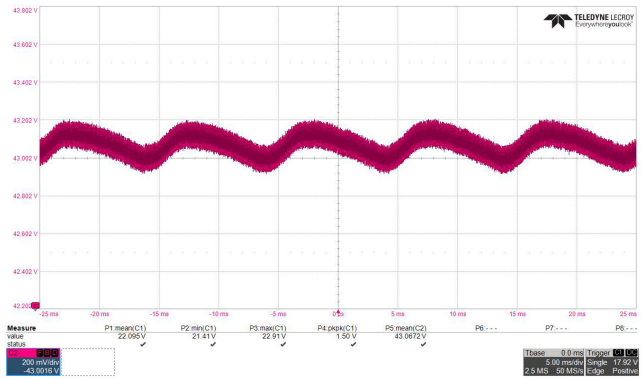

Fig. 18. Output voltage waveform due to source voltage fluctuations, fluctuations frequency $f = 100$ Hz. Each vertical division is 0.2 V, and each horizontal division is 5 ms.

TABLE IV
EXPERIMENTAL AND ANALYTICAL RESULTS COMPARISON

Description	Analysis	Experimental
Output voltage V_{out}[V]	43	42.98
Desired Switching frequency f[kHz]	50	49.33
Output voltage upper boundary envelop (AM&prop) [V]	0.0395	0.0425
Output voltage lower boundary envelop (AM&prop) [V]	0.0380	0.0412

Table IV. The source voltage fluctuations which are the result of rectification of the ac voltage signal are not purely sinusoidal as given in (16). Therefore, there exists some differences between analytical and experimental results.

VIII. CONCLUSION

An analytical method for analysis of the dynamics and performance of SMC dc–dc boost converter through LPRS method is proposed in the article. To the best knowledge of the authors, the provided analysis is the first example of application of the LPRS method to an application that involves a nonlinear plant model. The LPRS provides exact values of the frequency and amplitude of chattering (ripple/oscillations) in the output voltage and current, as well as, it enables analysis of source voltage fluctuation effect (which may be the result of ac voltage rectification) on the output voltage and current waveform via the equivalent gain concept. The LPRS analysis of source voltage fluctuations is done as a combination of the effects of AM and input signal propagation. The presented hardware experiments and simulation results support all aspects of the proposed LPRS analysis. The described characteristics of the LPRS methodology make this method a superior tool of analysis of SM dc–dc boost converter.

REFERENCES

[1] M. H. Rashid, *Power Electronics: Devices, Circuits, and Applications*, 4th Ed. London, U.K.: Pearson, 2014.
[2] V. Utkin, J. Guldner, and J. Shi, *Sliding Mode Control in Electro-Mechanical Systems*. Boca Raton, FL, USA: CRC Press, 2009.
[3] V. I. Utkin, *Sliding Modes in Control and Optimization*. Berlin, Germany: Springer Science & Business Media, 2013.

[4] J.-J. E. Slotine and W. Li, *Applied Nonlinear Control*. Englewood Cliffs, NJ, USA: Prentice Hall, 1991.
[5] Y. Shtessel, C. Edwards, L. Fridman, and A. Levant, *Sliding Mode Control and Observation*. Cambridge, MA, USA: Birkhauser, 2014.
[6] K. D. Young, V. I. Utkin, and U. Ozguner, "A control engineer's guide to sliding mode control," *IEEE Trans. Control Syst. Technol.*, vol. 7, no. 3, pp. 328–342, May 1999.
[7] K. D. Young, "Controller design for a manipulator using theory of variable structure systems," *IEEE Trans. Syst., Man, Cybern.*, vol. 8, no. 2, pp. 101–109, Feb. 1978.
[8] V. I. Utkin, "Sliding mode control design principles and applications to electric drives," *IEEE Trans. Ind. Electron.*, vol. 40, no. 1, pp. 23–36, Feb. 1993.
[9] S. Tan, Y. M. Lai, and C. K. Tse, "General design issues of sliding-mode controllers in DC-DC converters," *IEEE Trans. Ind. Electron.*, vol. 55, no. 3, pp. 1160–1174, Mar. 2008.
[10] E. Vidal-Idiarte, L. Martinez-Salamero, F. Guinjoan, J. Calvente, and S. Gomariz, "Sliding and fuzzy control of a boost converter using an 8-bit microcontroller," *IEE Proc. Electric Power Appl.*, vol. 151, no. 1, pp. 5–11, Jan. 2004.
[11] Siew-Chong Tan, Y. M. Lai, C. K. Tse, and M. K. H. Cheung, "Adaptive feedforward and feedback control schemes for sliding mode controlled power converters," *IEEE Trans. Power Electron.*, vol. 21, no. 1, pp. 182–192, Jan. 2006.
[12] E. Mamarelis, G. Petrone, and G. Spagnuolo, "Design of a sliding-mode-controlled SEPIC for PV MPPT applications," *IEEE Trans. Ind. Electron.*, vol. 61, no. 7, pp. 3387–3398, Jul. 2014.
[13] A. Reatti, F. Corti, A. Tesi, A. Torlai, and M. K. Kazimierczuk, "Effect of parasitic components on dynamic performance of power stages of DC-DC PWM buck and boost converters in CCM," in *Proc. IEEE Int. Symp. Circuits Syst.*, May 2019, pp. 1–5.
[14] A. Reatti, F. Corti, A. Tesi, A. Torlai, and M. K. Kazimierczuk, "Nonlinear exact analysis and solution of power stage of DC-DC PWM boost converter," in *Proc. IEEE Int. Symp. Circuits Syst.*, May 2019, pp. 1–5.
[15] R. Silva-Ortigoza, V. M. Hernandez-Guzman, M. Antonio-Cruz, and D. Munoz-Carrillo, "DC/DC buck power converter as a smooth starter for a DC motor based on a hierarchical control," *IEEE Trans. Power Electron.*, vol. 30, no. 2, pp. 1076–1084, Feb. 2015.
[16] L. Martinez-Salamero, A. Cid-Pastor, A. E. Aroudi, R. Giral, J. Calvente, and G. Ruiz-Magaz, "Sliding-mode control of DC-DC switching converters," *IFAC Proc. Volumes*, vol. 44, no. 1, pp. 1910–1916, 2011.
[17] R. Haroun, A. E. Aroudi, A. Cid-Pastor, G. Garcia, C. Olalla, and L. Martinez-Salamero, "Impedance matching in photovoltaic systems using cascaded boost converters and sliding-mode control," *IEEE Trans. Power Electron.*, vol. 30, no. 6, pp. 3185–3199, Jun. 2015.
[18] J. Yang, S. Li, and X. Yu, "Sliding-mode control for systems with mismatched uncertainties via a disturbance observer," *IEEE Trans. Ind. Electron.*, vol. 60, no. 1, pp. 160–169, Jan. 2013.
[19] E. Vidal-Idiarte, C. E. Carrejo, J. Calvente, and L. Martinez-Salamero, "Two-loop digital sliding mode control of DC-DC power converters based on predictive interpolation," *IEEE Trans. Ind. Electron.*, vol. 58, no. 6, pp. 2491–2501, Jun. 2011.
[20] A. Dashtestani and B. Bakkaloglu, "A fast settling oversampled digital sliding-mode DC-DC converter," *IEEE Trans. Power Electron.*, vol. 30, no. 2, pp. 1019–1027, Feb. 2015.
[21] B. A. Martinez-Trevino, A. El Aroudi, E. Vidal-Idiarte, A. Cid-Pastor, and L. Martinez-Salamero, "Sliding-mode control of a boost converter under constant power loading conditions," *IET Power Electron.*, vol. 12, no. 3, pp. 521–529, 2019.
[22] L. Albiol-Tendillo, E. Vidal-Idiarte, J. Maixe-Altes, S. Mendez-Prince, and L. Martinez-Salamero, "Seamless sliding-mode control for bidirectional boost converter with output filter for electric vehicles applications," *IET Power Electron.*, vol. 8, no. 9, pp. 1808–1816, 2015.
[23] R. P. Severns and G. Bloom, *Modern DC-to-DC Switchmode Power Converter Circuits*. Berlin, Germany: Springer, 1985.
[24] N. Mohan, T. M. Undeland, and W. P. Robbins, *Power Electronics: Converters, Applications, and Design*. Hoboken, NJ, USA: Wiley, 2003.
[25] R. D. Middlebrook and S. Cuk, "A general unified approach to modelling switching-converter power stages," in *Proc. IEEE Power Electron. Specialists Conf.*, Jun. 1976, pp. 18–34.
[26] P. Mattavelli, L. Rossetto, and G. Spiazzi, "Small-signal analysis of DC-DC converters with sliding mode control," *IEEE Trans. Power Electron.*, vol. 12, no. 1, pp. 96–102, Jan. 1997.
[27] D. Atherton, *Nonlinear Control Engineering-Describing Function Analysis and Design, Workingham, Berks*. New York, NY, USA: Van Nostrand, 1975.
[28] I. Boiko, *Discontinuous Control Systems: Frequency-Domain Analysis and Design*. Berlin, Germany: Springer Science & Business Media, 2009.
[29] I. Boiko, "Oscillations and transfer properties of relay servo systems–The locus of a perturbed relay system approach," *Automatica*, vol. 41, no. 4, pp. 677–683, 2005.
[30] I. Boiko, "Analysis of closed-loop performance and frequency-domain design of compensating filters for sliding mode control systems," *IEEE Trans. Autom. Control*, vol. 52, no. 10, pp. 1882–1891, Oct. 2007.
[31] I. Boiko, "LPRS analysis of sliding mode buck converter," *J. Franklin Inst.*, vol. 353, no. 18, pp. 5137–5150, 2016.
[32] R. Rafiezadeh and R. Grino, "A relay controller with parallel feed-forward compensation for a buck converter feeding constant power loads," in *Proc. 24th IEEE Int. Conf. Emerg. Technol. Factory Autom.*, Sep. 2019, pp. 445–452.
[33] L. Benadero, F. Torres, E. Ponce, and A. E. Aroudi, "Dynamic analysis of self-oscillating H-bridge inverters with state feedback," *J. Franklin Inst.*, vol. 357, no. 1, pp. 494–521, 2020.
[34] A. AlZawaideh and I. Boiko, "LPRS analysis of sliding mode control of a boost converter," in *Proc. 15th Int. Workshop Variable Struct. Syst.*, Jul. 2018, pp. 461–463.
[35] A. AlZawaideh and I. Boiko, "Analysis of a sliding mode boost converter under fluctuating input source voltage, using LPRS method," *Control Eng. Pract.*, vol. 92, 2019, Art. no. 104132.
[36] V. Utkin, "Sliding mode control of DC/DC converters," *J. Franklin Inst.*, vol. 350, no. 8, pp. 2146–2165, 2013.
[37] B. J. Cardoso, A. F. Moreira, B. R. Menezes, and P. C. Cortizo, "Analysis of switching frequency reduction methods applied to sliding mode controlled DC-DC converters," in *Proc. '92 7th Annu. Appl. Power Electron. Conf. Expo.*, Feb. 1992, pp. 403–410.
[38] P. Mattavelli, L. Rossetto, G. Spiazzi, and P. Tenti, "General-purpose sliding-mode controller for DC/DC converter applications," in *Proc. IEEE Power Electron. Specialist Conf.*, Jun. 1993, pp. 609–615.
[39] Siew-Chong Tan, Y. M. Lai, M. K. H. Cheung, and C. K. Tse, "On the practical design of a sliding mode voltage controlled buck converter," *IEEE Trans. Power Electron.*, vol. 20, no. 2, pp. 425–437, Mar. 2005.

Ayman AlZawaideh (Member, IEEE) received the B.Sc. and M.Sc. degrees in electrical engineering from Khalifa University, Abu Dhabi, United Arab Emirates, in 2015 and 2017, respectively.

He is currently a Research Associate with Khalifa University. His research interests include power converters, analysis and design of nonlinear systems, sliding mode control, and controller tuning.

Igor M. Boiko (Senior Member, IEEE) received the M.Sc. and Ph.D. degrees from Tula State University, Russia, in 1984 and 1990, respectively, and the D.Sc. degree from Higher Attestation Commission, Russia, in 2009.

He was with Tula State University, worked as a practitioner in the areas of process control and distributed control systems in Canada, and was with the Petroleum Institute, Abu Dhabi, United Arab Emirates. Currently, he is a Professor with Khalifa University of Science and Technology, Abu Dhabi, United Arab Emirates. He authored and coauthored four books on control theory and applications. His research interests include frequency-domain methods of analysis and design of nonlinear systems and sliding mode control systems, in particular, control of power converters, controller tuning, mechatronics, and process control applications.

Dr. Boiko is a member of the IEEE TC on variable-structure and sliding mode control. He is a Professional Engineer in Alberta, Canada.